Optically pumped terahertz laser based on intersubband transitions in a GaN/AlGaN double quantum well

N. Vukmirović, V. D. Jovanović, D. Indjin, Z. Ikonić, P. Harrison

School of Electronic and Electrical Engineering,

University of Leeds, Leeds LS2 9JT, United Kingdom

V. Milanović

School of Electrical Engineering, Bulevar kralja Aleksandra 73,

11120 Belgrade, Serbia and Montenegro

Abstract

A design for a GaN/AlGaN optically pumped terahertz laser emitting at $34\mu m$ ($\Delta E \sim 36$ meV) is presented. This laser uses a simple three-level scheme where the depopulation of the lower laser level is achieved via resonant longitudinal optical phonon emission. The quasi-bound energies and associated wave functions are calculated with the intrinsic electric field induced by the piezoelectric and the spontaneous polarization. The structures based on a double quantum well were simulated and the output characteristics extracted using a fully self-consistent rate equation model with all relevant scattering processes included. Both electron-longitudinal optical phonon and electron-acoustic phonon interactions were taken into account. The carrier distribution in subbands was assumed to be Fermi Dirac-like, with electron temperature equal to the lattice temperature, but with different Fermi levels for each subband. A population inversion of 12% for a pumping flux $\Phi = 10^{27}$ cm^{-2}s^{-1} at room temperature was calculated for the optimized structure. By comparing the calculated modal gain and estimated waveguide and mirror losses the feasibility of laser action up to room temperature is predicted.

I. INTRODUCTION

More than three decades have passed since the first proposal of a laser based on intersubband transitions in quantum wells[1]. Improvements in technology in the last decade have led to the realization of infrared intersubband lasers based on GaAs/AlGaAs and AlInAs/GaInAs and most recently on InAs/AlSb material systems. The electrically pumped or quantum cascade laser (QCL) from its first realization[2] has demonstrated an impressive and rapid development extending the emission wavelengths from the mid-infrared to the THz spectral range[3–9]. However, QCLs based on polar semiconductors such as GaAs/AlGaAs and AlInAs/GaInAs are not capable of emitting in the energy range around the longitudinal optical (LO) phonon energies ($E_{LO} \sim 36$ meV in GaAs and $E_{LO} \sim 34$ meV in InGaAs), leaving a gap in the spectral range between 30 and 40 μm. In comparison with QCLs, optically pumped intersubband lasers[10] have the disadvantage that an external pumping source is necessary. However, they offer the advantages of easier design and fabrication, higher selectivity in populating energy levels and a way of avoiding the free-carrier losses associated with contact regions.

Recently, intersubband transitions in GaN/AlGaN heterostructures started to attract the attention of researchers due to the prospect of their applications in optoelectronic devices. The large LO phonon energy and ultra-fast electron dynamics[11–13] offer a route for achieving the 30-40 μm terahertz region as the corresponding intersubband transitions are not influenced by the resonant electron-LO phonon interactions like in GaAs based systems[14]. The first design and theoretical investigations of a terahertz GaN/AlGaN QCL emitting in GaAs Reststrahlenband has been presented recently[15].

In this paper we present a design and a simulation of a GaN/AlGaN-based optically pumped far-infrared (THz) intersubband laser, emitting in the GaAs forbidden Reststralenband at 34 μm corresponding to a laser energy separation of 36 meV. This laser uses a simple three-level scheme shown in the inset of Fig. 1. Electrons from the ground state (subband 1) are optically pumped to the upper laser level (subband 3), while a fast depopulation of the lower laser level (subband 2) is achieved via resonant LO phonon emission. A detailed investigation of the possible population inversion and calculation of the output characteristics of proposed structure is also presented.

II. THEORETICAL MODEL

A. Electronic structure of a GaN/AlGaN multiple quantum well

Consider a GaN/AlGaN multiple quantum well consisting of N layers with widths $L_1, ..., L_N$, grown along the $z-$direction (Fig 1). The envelope function Schrödinger equation in effective mass approximation, in a system where a strong intrinsic electric field exists, is given as[16] (for in-plane wave vector $k_{||} = 0$):

$$-\frac{\hbar^2}{2}\frac{d}{dz}\left(\frac{1}{m(z)}\frac{d\eta}{dz}\right) + \left[x_i\Delta U + eF_i z + C_i\right]\eta(z) = E\eta(z), \tag{1}$$

where $m(z)$ is the parabolic effective mass (note that nonparabolicity was disregarded as the energies of corresponding states in this particular - terahertz design were not far above the conduction band edge), ΔU is the conduction band offset, F_i is the intrinsic polarization induced field in the i-th layer, and $C_i = C_{i-1} + e(F_{i-1} - F_i)L_{i-1}$ with the arbitrary taken $C_1 = 0$. The polarization-induced electric fields have been calculated using the expression[17]

$$F_j = \frac{\sum_{k=1}^{N}(P_k - P_j)\frac{L_k}{\varepsilon_k}}{\varepsilon_j \sum_{k=1}^{N}\frac{L_k}{\varepsilon_k}}, \tag{2}$$

where ε_i is the dielectric constant and P_i is the total polarization in i-th layer given as a sum of piezoelectric and spontaneous (pyroelectric) polarizations. The piezoelectric polarization was calculated as

$$P_{pz} = 2\frac{a - a_k}{a_k}\left(e_{31} - e_{33}\frac{C_{13}}{C_{33}}\right), \tag{3}$$

where C_{ij} are elastic constants, e_{ij} are piezoelectric constants, a_k is the lattice constant of the k-th layer, and a is the lattice constant of the buffer. In order to provide pseudomorphic growth, the buffer lattice constant (Al content in the buffer layer) has been chosen to satisfy the strain-balancing condition as in Ref. 16.

The spontaneous polarization was calculated with the bowing factor included:

$$P_{sp} = xP_{sp}^{AlN} + (1-x)P_{sp}^{GaN} - Cx(1-x), \tag{4}$$

where x is the molar content of AlN in the layer, $P_{sp}^{AlN} = -0.090$ C/m^2, $P_{sp}^{GaN} = -0.034$ C/m^2 and $C = -0.021$ C/m^2 (see Ref. 18).

Screening of piezoelectric and spontaneous polarization fields was not taken into account since it is small at the doping density (around 10^{11} cm^{-2}) and carrier densities considered

in this work, as shown in Ref. 19. We have also estimated that under such conditions the influence of many body effects[20] on transition energies is of the order of 1 meV, so these were neglected.

Since $m(z)$ is constant within a layer, an analytic treatment of equation (1) is possible. As the effective potential is stepwise linear, the two linearly independent solutions of the Schrödinger equation in each layer can be written in the form of Airy functions of the first and second kind[21].

B. Interaction of electrons with electromagnetic field

The fractional absorption on transitions from subband i to subband f is given by[22]:

$$A_{if}(\omega) = \frac{e^2\omega}{2\overline{n}\varepsilon_0 c}\int_0^\infty F_{if}(k_{||}^2)L(\hbar\omega,\hbar\omega_0)z_{if}^2 d(k_{||}^2), \tag{5}$$

where $\hbar\omega_0$ and $\hbar\omega$ are the transition and photon energies respectively, z_{if} is the dipole matrix element $z_{if} = \int \eta_i^* z \eta_f dz$, $\overline{n}$ is the refractive index in the GaN/AlGaN alloy, $k_{||}$ the in-plane wave vector, $F_{if}(k_{||}^2) = f_i(k_{||}^2) - f_f(k_{||}^2)$ the difference of occupancies of the two states and

$$L(\hbar\omega,\hbar\omega_0) = \frac{\Gamma}{2\pi}\frac{1}{(\hbar\omega-\hbar\omega_0)^2+(\Gamma/2)^2}, \tag{6}$$

the normalized Lorentzian, where Γ is the transition linewidth. In the case of parabolic subbands with the same effective mass the transition energy does not depend on $k_{||}$ and is equal to $\hbar\omega_0 = E_{f0} - E_{i0}$ (where E_{f0} and E_{i0} are energies of the bottoms of subbands f and i, respectively). Using the relation $1/(2\pi)\int_0^\infty f_i(k_{||}^2)d(k_{||}^2) = n_i$, where $n_i[\mathrm{cm}^{-2}]$ is the electron density in the $i-$th subband, it follows that

$$A_{if}(\omega) = \frac{e^2\omega\pi}{\overline{n}\varepsilon_0 c}z_{if}^2 L(\hbar\omega,\hbar\omega_0)(n_i - n_f), \tag{7}$$

where

$$\sigma_{if}(\omega) = \frac{e^2\omega\pi}{\overline{n}\varepsilon_0 c}z_{if}^2 L(\hbar\omega,\hbar\omega_0) \tag{8}$$

is the optical cross section.

C. Laser model

The rate equations for the three-level system were used to find the population inversion and the gain. These equations read:

$$\frac{dn_1}{dt} = -\sigma_{13}\Phi(n_1 - n_3) + W_{21}n_2 + W_{31}n_3 - W_{12}n_1 - W_{13}n_1, \tag{9}$$

$$\frac{dn_2}{dt} = W_{32}n_3 - W_{21}n_2 + W_{12}n_1 - W_{23}n_2, \tag{10}$$

$$\frac{dn_3}{dt} = \sigma_{13}\Phi(n_1 - n_3) - W_{31}n_3 - W_{32}n_3 + W_{13}n_1 + W_{23}n_2, \tag{11}$$

where $\Phi[\mathrm{cm}^{-2}\mathrm{s}^{-1}]$ is the pump flux, W_{ij} are the averaged transition rates between subbands i and j, evaluated by taking into account the in-plane wave vector dependence of the state occupancy (which is of Fermi-Dirac type and is inherent to the rate equations model) and of the transition rates, and $\sigma_{13} = \sigma_{13}(\omega = (E_{30} - E_{10})/\hbar)$ is the pump absorption cross section. The transition linewidth was taken to be equal to 15% of the transition energy, which is a typical value in the THz intersubband lasers[3–9].

In the calculation of the transition rates, the processes of emission and absorption of polar optical phonons, as well as acoustic phonons, were taken into account. Bulk-like phonon modes were assumed.

The transition rate for scattering an electron from initial state in subband i with in-plane wave vector k_i into any state in subband f (assuming the final state is empty) via the interaction with LO phonon is given by[23]:

$$W_{if}^{LO\mp}(k_i) = \frac{\Upsilon''\pi}{2}\Theta(k_i^2 - \frac{2m\Delta}{\hbar^2})\int_{-\infty}^{+\infty} \frac{|G_{if}(K_z)|^2 dK_z}{\sqrt{K_z^4 + 2K_z^2(2k_i^2 - \frac{2m\Delta}{\hbar^2}) + \left(\frac{2m\Delta}{\hbar^2}\right)^2}} \tag{12}$$

where $\Theta(x) = \begin{cases} 0 & x \le 0 \\ 1 & x > 0 \end{cases}$ is the step function, $\Upsilon'' = \frac{2me^2\omega_{LO}P'}{h^2}$, $P' = \left(N_0 + \frac{1}{2} \mp \frac{1}{2}\right)\left(\frac{1}{\varepsilon_\infty} - \frac{1}{\varepsilon_0}\right)$, the sign - corresponds to absorption, and + to emission, ω_{LO} is the LO phonon frequency, $\Delta = E_{f0} - E_{i0} \mp \hbar\omega_{LO}$, ε_∞ is the high frequency dielectric constant, ε_0 static dielectric constant, $N_0 = \left(\exp\frac{\hbar\omega_{LO}}{k_BT} - 1\right)^{-1}$ number of phonons with frequency ω_{LO} at a temperature T, and $G_{if}(K_z) = \int \eta_i(z)^* \exp(iK_z z)\eta_f(z)dz$ is the electron-phonon interaction form factor, while the transition rate for scattering via acoustic phonons is[23]:

$$W_{if}^{A\mp}(k_i) = \frac{D_A^2 m}{\rho v_s h^2}\int_0^\infty dK_z \int_0^{2\pi} d\phi |G_{if}(K_z)|^2 \frac{f(\alpha_1) + f(\alpha_2)}{\alpha_1 - \alpha_2}, \tag{13}$$

where

$$f(\alpha) = \Theta(\alpha)\alpha\sqrt{\alpha^2 + K_z^2}\left(N_0(\sqrt{\alpha^2 + K_z^2}) + \frac{1}{2} \mp \frac{1}{2}\right),$$

$N_0(K) = \left(\exp\frac{\hbar v_s K}{k_B T} - 1\right)^{-1}$, $\alpha_{1,2} = -k_i\cos\phi \pm \sqrt{(k_i\cos\phi)^2 - \frac{2m\Delta}{\hbar^2}}$, $\Delta = E_{f0} - E_{i0}$, D_A is the acoustic deformation potential, ρ the density, and v_s the longitudinal sound velocity. Equations (12) and (13) were derived under the assumption of parabolic subbands with the same effective mass m. This assumption will be justified later.

Transition rates calculated according to (12) and (13) were averaged across the subband with the effect of final-state blocking included, thus yielding:

$$\langle W_{if}^{LO\mp}\rangle = \frac{1}{2n_i\pi}\int_0^\infty d(k_i^2) W_{if}^{LO\mp}(k_i) f_{FD}(E_i(k_i), E_{Fi})\left[1 - f_{FD}(E_i(k_i) \pm \hbar\omega, E_{Ff})\right], \quad (14)$$

$$\langle W_{if}^{A\mp}\rangle = \frac{1}{2n_i\pi}\int_0^\infty d(k_i^2) W_{if}^{A\mp}(k_i) f_{FD}(E_i(k_i), E_{Fi})\left[1 - f_{FD}(E_i(k_i), E_{Ff})\right]. \quad (15)$$

It was assumed that the distribution of electrons in each subband is a Fermi-Dirac distribution with the electron temperature equal to the lattice temperature, but with different Fermi levels for each subband (E_{Fi} for subband i). Finally, we get an expression for the average transition rates $W_{if} = \langle W_{if}^{LO-}\rangle + \langle W_{if}^{LO+}\rangle + \langle W_{if}^{A-}\rangle + \langle W_{if}^{A+}\rangle$.

It is well known that electron-electron scattering becomes relevant only at high carrier concentration and at small spacings (up to about 10 meV) between energy levels[23], hence it should not be too important in the system considered here (this is checked for in section III).

Equations (9)-(10), together with the condition $n_s = n_1 + n_2 + n_3$ (n_s is the total electron density determined from electroneutrality of the structure), can be solved in the stationary case ($\frac{d}{dt} = 0$) to find the electron densities in the subbands. Unfortunately, the transition rates, as we have seen, depend on the population of subbands, therefore a self-consistent treatment is necessary with an initial guess for the subband populations. The Fermi levels are then obtained from

$$E_{Fi} = E_{i0} + k_B T \ln\left(\exp\frac{\pi\hbar^2 n_i}{m k_B T} - 1\right). \quad (16)$$

The transitions rates are then calculated according to (14)-(15) and the new electron densities are obtained from (9)-(10) and the electroneutrality condition. This step is repeated until the desired convergence is obtained. In our case, electron densities for the case of thermodynamic equilibrium are taken as a starting point for the self-consistent iteration and the procedure is repeated until the subband populations converge to within 1%.

Knowing the populations of the subbands it is easy to calculate the gain for stimulated emission, which is given by $g = A_{32}/L_W$, i.e. (see Eqs. 7 and 8):

$$g = \sigma_{23}\frac{n_3 - n_2}{L_W}, \tag{17}$$

where $\sigma_{23} = \sigma_{23}(\omega = (E_{30} - E_{20})/\hbar)$ is the lasing transition cross-section and L_W is the effective width of the quantum well structure.

III. RESULTS

A range of double quantum wells with $Al_xGa_{1-x}N$ barriers with the same x, and GaN wells were investigated. The length of the outer barriers was set to a fixed value of 100 Å, while the inner barrier width L_b, left and right well widths L_{w1} and L_{w2}, and the AlN content in the barriers x, were varied.

Firstly, x was varied in the interval $[0.1, 1]$ with a 0.1 step, and L_{w1}, L_{w2} and L_b in the interval $[10, 55]$ Å with a 5 Å step. We concluded that, as one might have expected, for $x \geq 0.2$ there are practically no structures with the desired spacings between the subbands $E_{30} - E_{20} \approx 36$ meV and $E_{20} - E_{10} \approx 91.2$ meV. At this point we can justify the assumption underlying equations (12) and (13). Since $m_{GaN} = 0.20\, m_0$, and $m_{AlN} = 0.30\, m_0$, for $x \in [0, 0.2]$ the effective mass in the $Al_xGa_{1-x}N$ layer takes values from the interval $[0.20\, m_0, 0.22\, m_0]$. This means that its variation across the structure is small and therefore it may be considered almost constant, implying parabolic subbands with the same effective mass.

Secondly, x was varied in the interval $[0.005, 0.200]$ with a 0.005 step, and L_{w1}, L_{w2} and L_b in the interval $[10, 95]$ Å with a 5 Å step. A range of structures having $32\,\text{meV} \leq E_{30} - E_{20} \leq 40\,\text{meV}$ and $83\,\text{meV} \leq E_{20} - E_{10} \leq 99\,\text{meV}$, were chosen for further analysis. For all those structures, the modal gain defined as $G_m = \sigma_{23}(n_3 - n_2)$ was calculated, with the desire to find the structure with the maximal modal gain. The calculation was performed at $T = 77$ K, with a doping concentration ($n_s = N_D L_W$) of $N_D = 3 \times 10^{16}\,\text{cm}^{-3}$, while the pump flux was varied in the interval $10^{21} - 10^{30}\,\text{cm}^{-2}\text{s}^{-1}$ with one decade step. When the flux is less than $10^{21}\,\text{cm}^{-2}\text{s}^{-1}$, none of the chosen structures had positive gain. At higher fluxes, the structure with $x = 0.070$, $L_{w1} = 90$ Å, $L_b = 15$ Å, $L_{w2} = 35$ Å is optimal in the range $10^{22} - 10^{27}\,\text{cm}^{-2}\text{s}^{-1}$ and was chosen for further analysis.

The profile of the conduction band edge of the chosen structure, as well as energy levels and the wave function moduli are given in figure 1.

Table 1 shows the values of the calculated average transition rates via interaction with LO and acoustic phonons for $\Phi = 10^{27}\,\mathrm{cm^{-2}s^{-1}}$ and $T = 77\,\mathrm{K}$. Our calculations show that these rates depend on the flux very weakly, meaning that these values can be considered as typical at $T = 77\,\mathrm{K}$. It is interesting to note that for the $3 \rightarrow 2$ transition the interaction with the acoustic phonon is dominant since the LO phonon emission is suppressed (the electron from the bottom of the third subband can not emit an LO phonon due to energy conservation).

Figure 2 shows the temperature dependence of the average transition rates from the higher to the lower subband. Transition rates from the lower to the higher subbands, not shown on the graph, grow significantly with temperature, since they are proportional to the number of phonons which also increases. Transition rate $3 \rightarrow 2$ also rises with temperature. In the low temperature range this rise is mainly caused by the increase in number of acoustic phonons, while at higher temperatures it rises because the LO phonon emission rate becomes less suppressed. However, transition rates $3 \rightarrow 1$ and $2 \rightarrow 1$ don't increase with temperature, they even show a slight decrease. This is caused by the fact that the term N_0+1 is practically constant with temperature, while at higher temperatures more electrons have higher in-plane wave vectors and thus slightly smaller transition rates.

In order to check our assumption about the relevance of electron-electron scattering we have included it in the calculation of the gain for the chosen structure at $\Phi = 10^{27}\,\mathrm{cm^{-2}s^{-1}}$ and two temperatures, $T = 77\,\mathrm{K}$ and $T = 300\,\mathrm{K}$. In both cases, including electron-electron scattering changes the gain by only about 1%, which justifies neglecting it altogether.

The pumping flux dependence of the subband populations and gain is shown in figure 3. When the flux is low (around $\Phi = 10^{21}\,\mathrm{cm^{-2}s^{-1}}$) n_2 is greater than n_3 and there is no population inversion. At slightly higher flux (around $\Phi = 10^{22}\,\mathrm{cm^{-2}s^{-1}}$) population inversion occurs. In the next part of the graph we see that $n_3 \gg n_2$ and that n_3 is linearly dependent on the flux. Finally, at $\Phi \approx 10^{28}\,\mathrm{cm^{-2}s^{-1}}$, n_3 approaches n_1 and the graph reaches saturation. In the range from $\Phi = 10^{23}\,\mathrm{cm^{-2}s^{-1}}$ to $\Phi = 10^{27}\,\mathrm{cm^{-2}s^{-1}}$ the gain depends linearly on the flux, and then saturates (as well as n_3, this is expected since in that region $n_3 \gg n_2$ so that gain is proportional to n_3).

Figure 4 shows the temperature dependence of the electron densities and the gain. As expected, the gain decreases with temperature. However, as the LO phonon energy is

considerably higher than the lasing energy, the undesirable LO phonon emission is suppressed resulting in only a slight decrease of the gain.

Finally, we discuss the possibility of the laser action by comparing the gain with estimated values of the waveguide losses. The waveguide design assumed here is based on a single-surface plasmon configuration with the gold top and highly doped thin GaN bottom contact layer, see Fig. 5, similar to that implemented in the recently reported terahertz QCLs[6]. To find the mode intensity pattern and the propagation losses we used a numerical calculation based on the transfer matrix method[24] with a wavelength dependent complex dielectric permittivity parameterized via the Drude model. We assumed the doping density of the 0.15 μm thick bottom contact layer to be $5 \times 10^{19}\,\mathrm{cm}^{-3}$ and around 130 periods of the designed optically pumped structure in the active region. The waveguide losses are calculated to be $\alpha_{\mathrm{W}} \approx 23\ \mathrm{cm}^{-1}$ and the mode confinement $\Gamma = 0.40$. We have estimated the mirror losses, using $\alpha_M = -1/(2L)\ln R$, to be around 2 cm^{-1}, which gives the overall effective losses factor to be around $(\alpha_W + \alpha_M)/\Gamma \approx 62\ \mathrm{cm}^{-1}$, less than the calculated gain for the pumping flux of $\Phi = 10^{27}\ \mathrm{cm}^{-2}\mathrm{s}^{-1}$, even at room temperature (see Fig. 4).

IV. CONCLUSION

In this paper, a prototype for an optically pumped intersubband THz laser emitting at $\lambda \approx 34\mu$m (36 meV i.e. in GaAs Reststrahlen region) based on a GaN/AlGaN double quantum well as an active region was proposed. The intersubband rate equations were solved self-consistently with both the LO and acoustic phonon transition rates taken into account. A design with the maximal modal gain among the investigated structures was selected for further analysis of flux and temperature dependence of gain. At $T = 77$ K values of gain of around 100 cm^{-1} at flux of $10^{27}\ \mathrm{cm}^{-2}\mathrm{s}^{-1}$ are predicted. A suitable waveguide design was presented, and losses and confinement factor calculated. For the designed structure the feasibility of lasing action even at room temperature is predicted by comparing the calculated modal gain with estimated waveguide and mirror losses.

[1] R. F. Kazarinov and R. A. Suris, Sov. Phys. Semicond. **5**, 707 (1971).

[2] J. Faist, F. Capasso, D. L. Sivco, C. Sirtori, A. L. Hutchinson, and A. Y. Cho, Science **264**, 553 (1994).

[3] F. Capasso, R. Paiella, R. Martini, R. Colombelli, C. Gmachl, T.L. Myers, M.S. Taubman, R.M. Williams, C.G. Bethea, K. Unterrainer, H.Y. Hwang, D.L. Sivco, A.Y. Cho, A.M. Sergent, H.C. Liu and E.A. Whittaker, IEEE J. Quantum Electr., **38**, 511 (2002).

[4] R. Köhler, A. Tredicucci, F. Beltram, H. E. Beer, E. H. Linfield, A. G. Davies, D. A. Ritchie, R. C. Iotti, F. Rossi, Nature **417**, 156 (2002).

[5] B.S. Williams, S. Kumar, Q. Hu, and J. L. Reno, Electr. Lett. **40**, (2004).

[6] G. Scalari, L. Ajili, J. Faist, H. Beere, E. Linfield, D. Ritchie, G. Davies, Appl. Phys. Lett. **82** 3165 (2003).

[7] B.S. Williams, S. Kumar, H. Callebaut, Q. Hu, and J. L. Reno, Appl. Phys. Lett. **83**, 5142 (2003).

[8] S. Kumar, B.S. Williams, S. Kohen, Q. Hu, and J. L. Reno, Appl. Phys. Lett. **84**, 2494 (2004).

[9] S. Barbieri, J. Alton, H. E. Beer, J. Fowler, E. H. Linfield, and D. A. Ritchie, Appl. Phys. Lett. **85**, 1674 (2004).

[10] O. Gauthier-Lafaye, P. Boucaud, F. H. Julien, S. Sauvage, S. Cabaret, J. M. Lourtioz, V. Thierry-Mieg, and R. Planel, Appl. Phys. Lett. **71**, 3619 (1997).

[11] N. Iizuka, K. Kaneko, N. Suzuki, T. Asano, S. Noda, and O. Wada, Appl. Phys. Lett. **77**, 648 (2000).

[12] J. D. Heber, C. Gmachl, H. M. Ng, and A. Y. Cho, Appl. Phys. Lett. **81**, 1237 (2002).

[13] C. Gmachl, S. V. Frolov, H. M. Ng, S.-N. G. Chu, and A. Y. Cho, Electron. Lett. **37**, 378 (2001).

[14] D. Indjin, P. Harrison, R. W. Kelsall, Z. Ikonić, Appl. Phys. Lett., **82**, 1347 (2003).

[15] V. D. Jovanović, D. Indjin, Z. Ikonić, P. Harrison, Appl. Phys. Lett., **84**, 2995 (2004).

[16] V. Jovanović, Z. Ikonić, D. Indjin, P. Harrison, V. Milanović, and R. Soref, J. Appl. Phys. **93**, 3194 (2003).

[17] F. Bernardini and V. Fiorentini, Phys. Status Solidi B **216**, 391 (1999).

[18] I. Vurgaftman and J. R. Meyer, J. Appl. Phys. **94**, 3675 (2003).

[19] V. Fiorentini and F. Bernardini, Phys. Rev. B **60**, 8849 (1999).

[20] H. C. Liu and A. J. SpringThorpe, Phys. Rev. B **61**, 15629 (2000).

[21] M. Abramowitz and I. Stegun, *Handbook of Mathematical Functions* (Dover Publications, New York, 1965).

[22] V. Jovanović, D. Indjin, Z. Ikonić, V. Milanović and J. Radovanović, Solid State Commun. **121**, 619 (2002).

[23] P. Harrison, Quantum Wells, Wires and Dots, John Wiley and Sons Ltd., Chichester, England, 2000.

[24] E. Anemogiannis, E. N. Glytsis, T. K. Gaylord, IEEE J. Lightwave Technol. **17**, 929 (1999).

Figure captions

FIG. 1: Conduction band profile, energy levels and wave function moduli for the structure $x = 0.070$, $L_{w1} = 90$ Å, $L_b = 15$ Å, $L_{w2} = 35$ Å. The inset shows the three-level scheme of this laser: electrons from the ground state (subband 1) are optically pumped to the upper laser level (subband 3), while a fast depopulation of the lower laser level (subband 2) is achieved via resonant LO phonon emission.

FIG. 2: Temperature dependence of average transition rates at $\Phi = 10^{27}$ cm^{-2}s^{-1} for the structure from Fig. 1

FIG. 3: Flux dependence of electron densities (left axis), gain (right axis) and effective losses factor at $T = 77$ K for the structure from Fig. 1

FIG. 4: Temperature dependence of electron densities and gain at $\Phi = 10^{27}$ cm^{-2}s^{-1} for the structure from Fig. 1

FIG 5: Single-plasmon waveguide design and mode profile. Total thickness of active region is 4.5μm ($\sim$ 130 periods of structure). The 0.15μm thick bottom contact layer is assumed to be doped with 5×10^{19}cm^{-3}

Figures

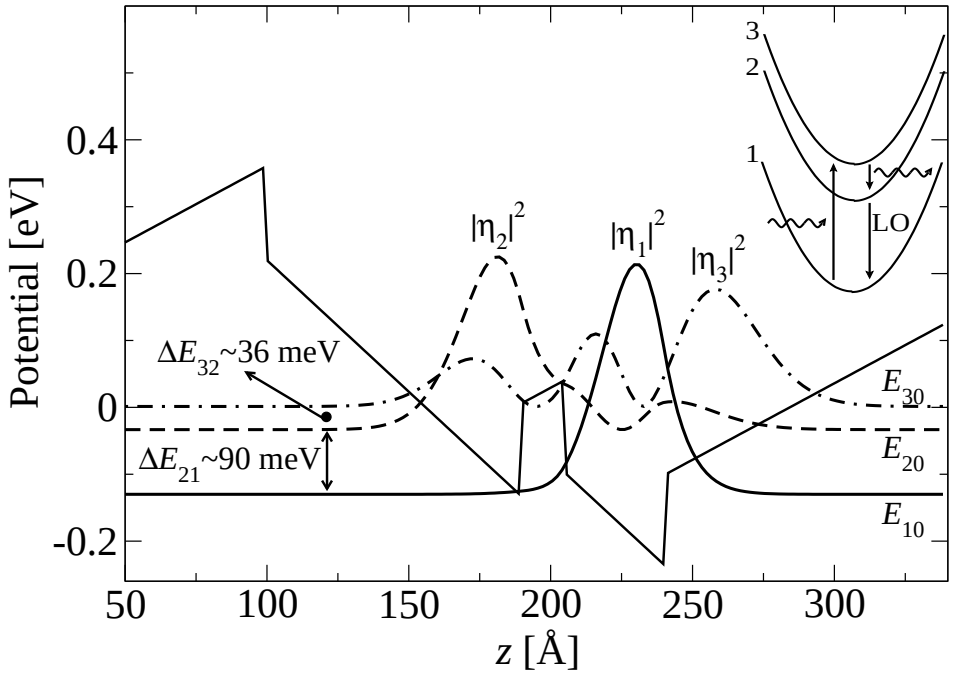
Potential [eV]
0.4
0.2
0
-0.2
50
100
150
200
250
300
z [Å]
|η2|2
|η1|2
|η3|2
ΔE32~36 meV
ΔE21~90 meV
E30
E20
E10
3
2
1
LO

FIG. 1:

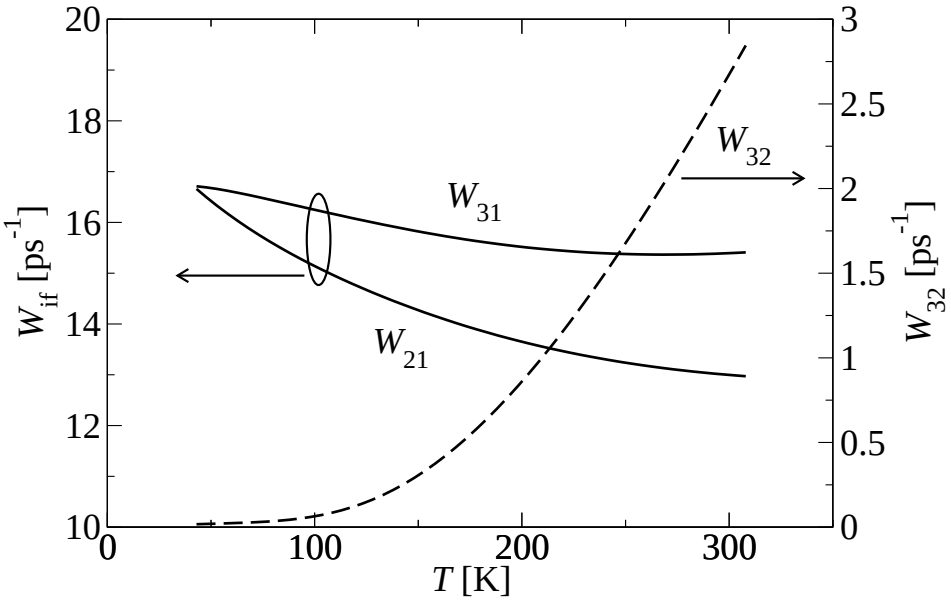
20
18
16
14
12
10
3
2.5
2
1.5
1
0.5
0
0
100
200
300
T [K]
W_if [ps^-1]
W_32 [ps^-1]
W_31
W_21
W_32

FIG. 2:

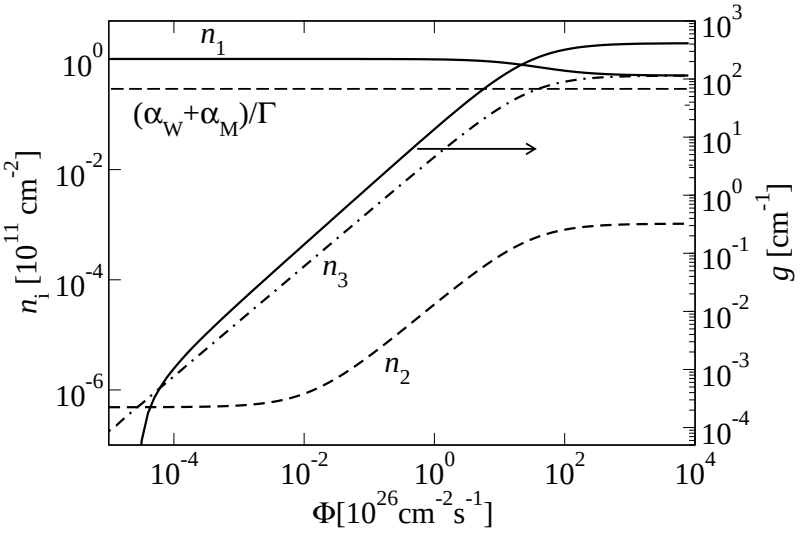
n_1
$(\alpha_W+\alpha_M)/\Gamma$
n_3
n_2
n_i [10^{11} cm^{-2}]
g [cm^{-1}]
Φ[10^{26}cm^{-2}s^{-1}]
10^{0}
10^{-2}
10^{-4}
10^{-6}
10^{3}
10^{2}
10^{1}
10^{0}
10^{-1}
10^{-2}
10^{-3}
10^{-4}
10^{-4}
10^{-2}
10^{0}
10^{2}
10^{4}

FIG. 3:

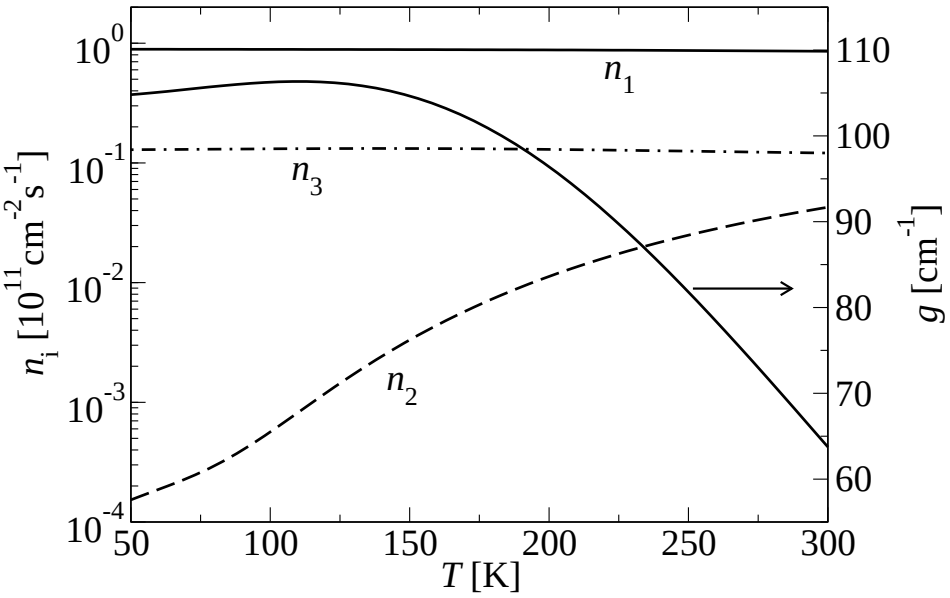
10^0
10^{-1}
10^{-2}
10^{-3}
10^{-4}
n_i [10^{11} cm^{-2} s^{-1}]
n_1
n_3
n_2
50
100
150
200
250
300
T [K]
110
100
90
80
70
60
g [cm^{-1}]

FIG. 4:

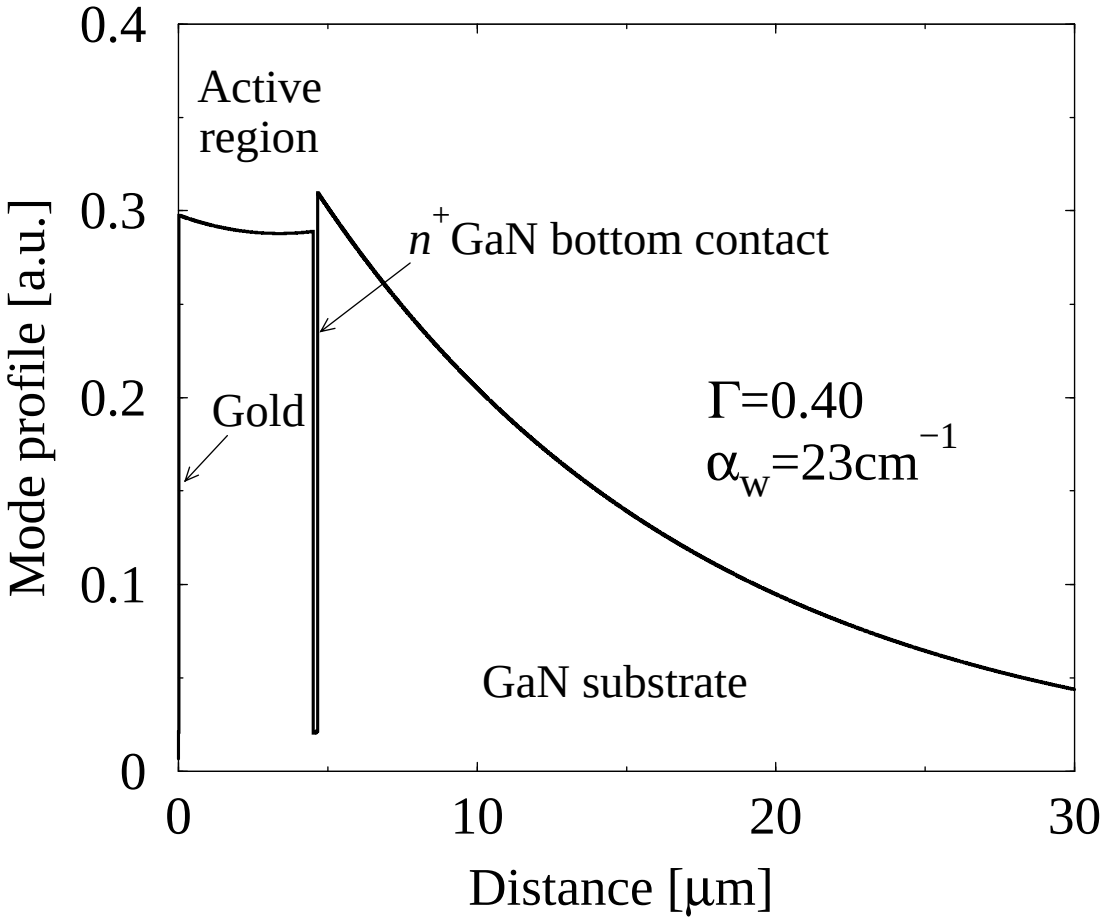
0.4
0.3
0.2
0.1
0
Mode profile [a.u.]
Active
region
n^+GaN bottom contact
Gold
Γ=0.40
α_w=23cm^{-1}
GaN substrate
0
10
20
30
Distance [μm]

FIG. 5:

Tables

TABLE 1: Average transition rates for interaction with longitudinal optical phonon (LO) and acoustic phonon (A) at $\Phi = 10^{27}\ \mathrm{cm}^{-2}\mathrm{s}^{-1}$ and $T = 77\ \mathrm{K}$

$\langle W \rangle [\mathrm{ps}^{-1}]$	$2 \to 1$	$3 \to 1$	$3 \to 2$
LO	15.64	16.43	0.0035
A	0.014	0.032	0.029
$\langle W \rangle [10^{-5}\ \mathrm{ps}^{-1}]$	$1 \to 2$	$1 \to 3$	$2 \to 3$
LO	0.73	0.0033	2.33
A	0.00061	0.0000077	13.2